IOPscience iopscience.iop.org

Home Search Collections Journals About Contact us My IOPscience

Treatment of solid tumors by interstitial release of recoiling short-lived alpha emitters

This content has been downloaded from IOPscience. Please scroll down to see the full text.

2007 Phys. Med. Biol. 52 5025

(http://iopscience.iop.org/0031-9155/52/16/021)

View the table of contents for this issue, or go to the journal homepage for more

Download details:

IP Address: 129.101.79.200
This content was downloaded on 15/08/2014 at 12:20

Please note that terms and conditions apply.

IOP Publishing Physics in Medicine and Biology

Phys. Med. Biol. **52** (2007) 5025–5042 doi:10.1088/0031-9155/52/16/021

Treatment of solid tumors by interstitial release of recoiling short-lived alpha emitters

L Arazi[1], T Cooks[2], M Schmidt[1], Y Keisari[2] and I Kelson[1]

[1] School of Physics and Astronomy, Raymond and Beverly Sackler Faculty of Exact Sciences, Tel Aviv University, Tel Aviv 69978, Israel
[2] Department of Human Microbiology, Sackler Faculty of Medicine, Tel Aviv University, Tel Aviv 69978, Israel

E-mail: kelson@post.tau.ac.il

Received 1 May 2007, in final form 23 June 2007
Published 1 August 2007
Online at stacks.iop.org/PMB/52/5025

Abstract

A new method utilizing alpha particles to treat solid tumors is presented. Tumors are treated with interstitial radioactive sources which continually release short-lived alpha emitting atoms from their surface. The atoms disperse inside the tumor, delivering a high dose through their alpha decays. We implement this scheme using thin wire sources impregnated with ^{224}Ra, which release by recoil ^{220}Rn, ^{216}Po and ^{212}Pb atoms. This work aims to demonstrate the feasibility of our method by measuring the activity patterns of the released radionuclides in experimental tumors. Sources carrying ^{224}Ra activities in the range 10–130 kBq were used in experiments on murine squamous cell carcinoma tumors. These included gamma spectroscopy of the dissected tumors and major organs, Fuji-plate autoradiography of histological tumor sections and tissue damage detection by Hematoxylin-Eosin staining. The measurements focused on ^{212}Pb and ^{212}Bi. The ^{220}Rn/^{216}Po distribution was treated theoretically using a simple diffusion model. A simplified scheme was used to convert measured ^{212}Pb activities to absorbed dose estimates. Both physical and histological measurements confirmed the formation of a 5–7 mm diameter necrotic region receiving a therapeutic alpha-particle dose around the source. The necrotic regions shape closely corresponded to the measured activity patterns. ^{212}Pb was found to leave the tumor through the blood at a rate which decreased with tumor mass. Our results suggest that the proposed method, termed DART (diffusing alpha-emitters radiation therapy), may potentially be useful for the treatment of human patients.

 © 2007 IOP Publishing Ltd Printed in the UK

1. Introduction

The efficacy of alpha particles against cancer cells is well established. Typically, only a few alpha particle hits to the cell nucleus are required to inactivate its proliferative capability (Hall 2000, Larsen *et al* 1998, Macklis *et al* 1992, Rotmensch *et al* 1989). In addition, compared to photons or electrons, the effect of alpha radiation is significantly less sensitive to the cell oxygenation state and position in the cell cycle (Hall 2000). The short range of alpha particles in tissue (40–90 μm) ensures that cells lying outside of the targeted region are spared. However, it also requires that the alpha emitting atoms are brought to the immediate vicinity of the target cancer cells, or be otherwise ineffective.

Work on the therapeutic utilization of alpha particles in the treatment of cancer has focused, in the last two decades, on targeted alpha therapy, recently reaching clinical trials. This includes a completed phase I trial for the treatment of bone metastases with ^{223}Ra (Nilsson *et al* 2005) and completed or ongoing alpha-radioimmunotherapy (α-RIT) trials, involving monoclonal antibodies or peptides labeled with ^{213}Bi or ^{211}At, for myeloid leukemia (Jurcic 2005), melanoma (Allen 2006), lymphoma (Schmidt *et al* 2004) and glioma (Kneifel 2006, Zalutsky 2005). Systemic α-RIT is generally considered to be best suited for treating isolated cells, small cell clusters and micrometastases, rather than solid tumors (Allen 2006, Couturier *et al* 2005, Kennel *et al* 1999, Mulford *et al* 2005, Zalutsky 2006). This is largely because of physical barriers in solid tumors (such as the elevated interstitial fluid pressure), which preclude efficient extravasation and further dispersion of the labeled targeting vectors throughout the tumor mass, leading, because of the short range of alpha particles, to highly irregular dose distributions (Christiansen and Rajasekaran 2004, Jain and Baxter 1988, Jain 1999, Larsen and Bruland 1998). Direct intratumoral injection of the labeled vectors can assist in bypassing such barriers, primarily those associated with the endothelium (Christiansen and Rajasekaran 2004). In particular, intralesional injection of monoclonal antibodies labeled with ^{213}Bi was shown to be effective in regressing melanoma lesions in both preclinical and clinical studies (Allen *et al* 2001, 2005).

In this paper we present a different and, in a sense, simpler approach for the application of alpha particles against solid tumors. The basic idea—here implemented using the ^{224}Ra decay chain—is to insert into the tumor a number of specially prepared radioactive sources, *which continually release short-lived alpha emitting atoms from their surface*. These atoms spread within the tumor by the combined effects of diffusion and convection (vascular and possibly interstitial), forming a region of tumor cell destruction, where a lethal dose is delivered through their alpha decays. Since, as in direct intratumoral injection, the alpha emitters begin their journey in the cellular space, rather than being conjugated to macromolecules that arrive at the tumor in the blood, and since no molecular targeting mechanism is involved, their subsequent distribution throughout the tumor may be expected to be less affected by the obstacles that hinder systemic α-RIT.

To be therapeutically relevant for the treatment of solid tumors, cell destruction must extend continuously a few millimeters from the source, two orders of magnitude larger than the alpha particle range in tissue. If this is the case, tumors may be treated by deploying a finite number of sources at a typical spacing of a few millimeters—much as in photon-based brachytherapy.

The aim of this paper is two-fold: first, to introduce the suggested concept and describe the practical means for its implementation; second, to demonstrate that the alpha emitting atoms released by the source indeed migrate to considerable distances within the tumor and lead to cell destruction over a region of several millimeters.

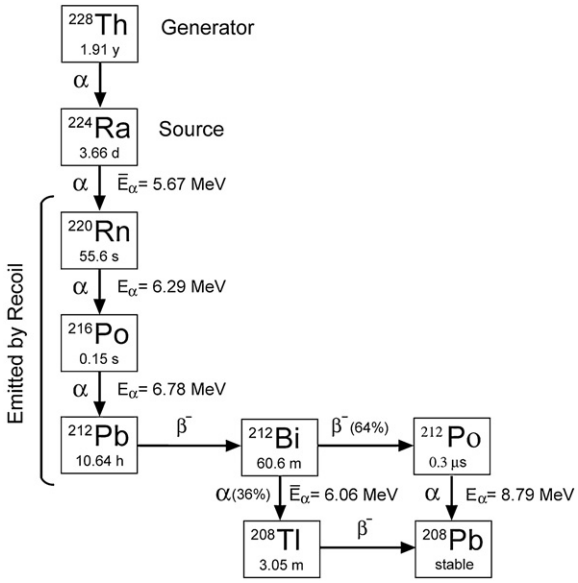

Figure 1. The ^{224}Ra decay chain.

We begin by describing the ^{224}Ra decay chain and its utilization and continue by outlining the source preparation and characterization procedures. We next discuss the dispersion of ^{224}Ra progeny throughout the tumor mass. The released radionuclides migration is treated by both theoretical and experimental techniques. A simplified scheme for estimating the absorbed dose is also presented. The experimental work reported herein focused on one particular model—murine squamous cell carcinoma (SCC) derived from the SQ2 cell line (Blank *et al* 2004). Due to the underlying principle of our method, we call it DART—diffusing alpha-emitters radiation therapy.

2. The DART source

2.1. Alpha emitters release mechanism

The diffusing atoms are released from the source by recoil: when a radioactive atom emits an alpha particle in one direction (with energy of 6–9 MeV), its daughter atom recoils in the opposite direction with a kinetic energy of about 100–170 keV. This energy is sufficiently large for the recoiling atom to traverse 10–20 nm in most solid materials. Thus, the source consists of parent alpha emitting atoms embedded closely below its surface, at a depth that prevents them from entering the tumor themselves, but allows considerable release of their recoiling daughters. These continually recoil into the tumor at a rate which decays exponentially with the parent isotope half-life.

2.2. The ^{224}Ra decay chain

To implement our idea, we chose the alpha decay chain beginning with ^{224}Ra (figure 1). The source—a thin conducting wire carrying a small activity of ^{224}Ra—is inserted through a fine-gauge needle into the tumor. Once inside the tumor and over a period determined by the

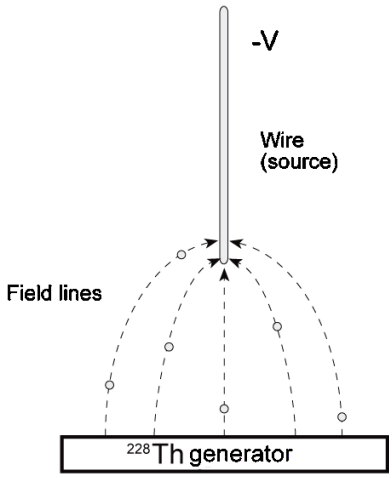

Figure 2. Schematic representation of the generator–source setup.

^{224}Ra half-life (3.66 d), the source releases, by recoil, ^{220}Rn (55.6 s half-life), ^{216}Po (0.15 s half-life) and ^{212}Pb (10.64 h half-life) atoms, while the remaining atoms of ^{224}Ra stay below its surface. ^{220}Rn, a noble gas, diffuses in the extra- and intra-cellular space near the source with no chemical interactions, occasionally entering and leaving the porous network of tumoral blood vessels. It contributes two alpha particles through its own decay and through that of its exceedingly short-lived daughter ^{216}Po, which disintegrates essentially at the same point. ^{212}Pb enters the tumor either by directly recoiling from the source or following the decay of ^{216}Po away from the source, giving rise to a third alpha particle: it beta-decays to ^{212}Bi (60.6 min half-life), which either alpha decays to ^{208}Tl (3.05 min half-life) or beta decays to ^{212}Po (0.3 μs half-life), which then alpha decays to stable ^{208}Pb (Lederer and Shirley 1977).

2.3. Source preparation

As ^{224}Ra is itself the result of the alpha decay of ^{228}Th (1.91 y half-life), the production of ^{224}Ra-bearing sources is based on the use of a ^{228}Th generator—a surface covered with a layer containing ^{228}Th, thin enough for substantial release of recoiling ^{224}Ra atoms. The generator–source setup (shown schematically in figure 2) comprises an electrically isolated, air-filled enclosure with the ^{228}Th generator at one end and a conducting wire, which serves as the injected source, at the other. The wire is held at a negative potential relative to the generator, concentrating the electrostatic field lines emerging from the generator surface near its tip. Positive ^{224}Ra ions recoiling out of the generator, with energies up to $\sim$100 keV, quickly thermalize by collisions with the air molecules and drift along the field lines to the wire, on whose surface they settle. To protect the highly reactive radium from being removed from the wire once inside the tissue, the wire is subsequently heated to induce radium diffusion away from the surface to a depth of several nanometers, which still allows considerable release of the alpha emitting daughters. The duration of the electrostatic collection stage, dictated by the 3.7 d half-life of ^{224}Ra, is of the order of a few days.

^{228}Th generators were prepared by evaporating a droplet of carrier-free 1M HCl solution containing up to 370 kBq $^{228}ThCl_4$ (Isotope Products Laboratories, Burbank, CA, USA), on a hydrophilic 4 cm^2 silicon surface, followed by heating in a vacuum to 800 $^\circ$C. This

yielded ^{228}Th layers with a ^{224}Ra desorption probability of 20–30% (i.e., for each decay of ^{228}Th there was a 20–30% probability that the recoiling ^{224}Ra atom would leave the surface). ^{228}Th activities were measured by standard solid state alpha particle spectroscopy. The ^{224}Ra desorption probability was found by measuring the buildup of ^{224}Ra on a stainless steel foil placed in proximity to the ^{228}Th generator in a vacuum.

Sources made of 0.3 mm diameter stainless steel acupuncture needles were prepared for the *in vivo* experiments described below according to the above procedure. The typical collection voltage was 2–3 kV and the typical distance between the ^{228}Th generator and the wire tip was 5–15 mm, with resulting ^{224}Ra collection efficiency of ∼95%. Once loaded with ^{224}Ra the wires were heated in a N_2 atmosphere to 450 °C, characterized by standard alpha spectroscopy and then repeatedly immersed in water and re-measured, until the radium loss to water became acceptably low (typically 1–2% of the source activity). The wires were then cut to their final length of 6 mm. ^{224}Ra activities of sources ranged from 10 to 130 kBq, with ^{220}Rn desorption probabilities of 30–43%.

3. ^{220}Rn diffusion—theoretical consideration

The physical feasibility of DART can be appreciated by considering the diffusion of ^{220}Rn, which governs the dose distribution related to the first two alpha particles emitted away from the source. Radon's inert nature makes it possible to estimate the dose profile resulting from its migration by a straightforward theoretical model. We assume that the migration of ^{220}Rn is purely diffusive, with a constant effective diffusion coefficient D_{Rn} and that all ^{220}Rn atoms are released from a point source at the origin, whose activity decays exponentially with ^{224}Ra half-life. By solving the time-dependent diffusion equation under these conditions (appendix A), the local activity of ^{220}Rn at any given point can be found for all times. An approximation for the absorbed dose distribution (from source insertion to infinity) is then found by time integration of the local activity, assuming that each decay of ^{220}Rn leads to two alpha particles depositing their energy locally, one contributed by ^{220}Rn and the other by ^{216}Po (this actually gives the local kerma, rather than the absorbed dose, but for the illustrative purpose of this discussion we neglect the difference between two). Since there are no published data for the effective diffusion coefficient of radon in tissue, we used two reference values: the diffusion coefficient of radon in water at 37 °C, 1.9×10^{-5} cm^2 s^{-1} (Jahne *et al* 1987), and, following the NRC report on radon in drinking water (NRC 1999), the effective diffusion coefficient of xenon in tissue, 0.5×10^{-5} cm^2 s^{-1}.

In what follows, we choose 10 Gy as a reference dose to estimate the size of the region affected by the source (we elaborate on this choice in the discussion section). Figure 3(a) shows the calculated ^{220}Rn/^{216}Po absorbed dose for a point source whose ^{220}Rn release rate at $t = 0$ is 37 kBq (1 μCi), for the above two values for the effective diffusion coefficient. Taking $D_{\mathrm{Rn}} = 1.9 \times 10^{-5}$ cm^2 s^{-1} results in the absorbed dose exceeding 10 Gy up to a radial distance of 2.6 mm from the source, while $D_{\mathrm{Rn}} = 0.5 \times 10^{-5}$ cm^2 s^{-1} leads to such a dose up to 1.7 mm away from it. Figure 3(b) shows the dependence of this distance on the source initial ^{220}Rn release rate, for the same diffusion coefficient values. Note the steep rise of the diameter at extremely low source activities, followed by the much milder slope for higher-activity sources. Keeping in mind that the decay point of ^{220}Rn is effectively the starting point for the migration of ^{212}Pb which may further distribute away from the source, this simple calculation demonstrates that the size of the region subject to alpha particle irradiation may indeed be expected to be of the order of millimeters rather than a few dozen microns. An experimental verification of this is given in the next section.

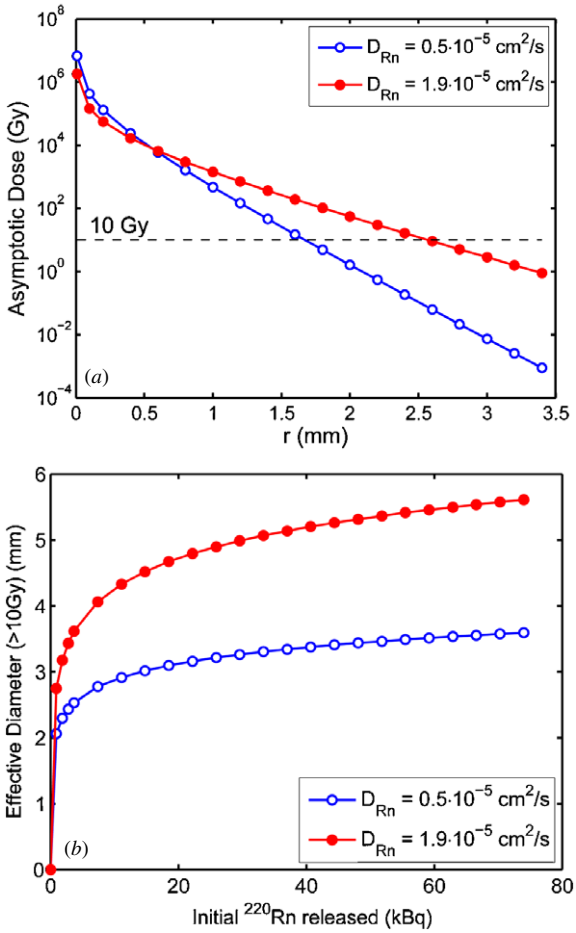

Figure 3. Results of simple diffusion calculations regarding the asymptotic dose delivered by ^{220}Rn and ^{216}Po away from a point source at the origin, for two reference values for radon's effective diffusion coefficient. (a) The dependence of the dose on the radial distance from a source releasing 37 kBq ^{220}Rn at $t = 0$. (b) The dependence of the diameter of the region receiving >10 Gy asymptotically on the source ^{220}Rn release rate.

4. *In vivo* measurements of ^{212}Pb/^{212}Bi distributions

4.1. General considerations

The third alpha particle emitted away from the source results from the decay of ^{212}Pb progeny—^{212}Bi and ^{212}Po. To estimate this component of the total dose, one must first study the transport of ^{212}Pb inside the tumor, and then the possible redistribution of ^{212}Bi relative to ^{212}Pb.

^{212}Pb, unlike radon, does interact chemically with surrounding molecules, in particular lead-binding proteins (Godwin 2001). Its subsequent redistribution throughout the tumor is governed by the transport of these proteins inside the cells, the extracellular space and the vascular network. ^{212}Pb-labeled proteins (and possibly free ^{212}Pb ions) entering the plasma are either captured by red blood cells or remain available for exchange with the surrounding tissue (Leggett 1993). ^{212}Pb entering viable vascular routes can thus be taken out of the tumor

and redistribute in various organs. This complicated picture apparently defies quantitative theoretical modeling. However, unlike ^{220}Rn, whose half-life is too short to allow for direct determination of its *in vivo* distribution, the half-life of ^{212}Pb is conveniently long to enable such measurements. Two experimental methods were implemented to determine ^{212}Pb spatial distribution inside treated tumors: one utilizing its gamma emissions, the other the alpha emissions of its progeny ^{212}Bi and ^{212}Po. Gamma spectroscopy was also used to measure the local ^{212}Bi/^{212}Pb activity ratio inside the tumor, as well as ^{212}Pb leakage from the tumor and subsequent uptake in various organs.

4.2. Experimental tumor model

In vivo measurements of ^{212}Pb and ^{212}Bi distributions were performed on murine squamous cell carcinoma (SCC) tumors derived from the SQ2 cell line, originating from a SCC tumor that had developed spontaneously in a male BALB/c mouse (Blank *et al* 2004). Cells were cultured in DMEM supplemented with 10% fetal calf serum, 2 mM L-glutamine, 100 U ml^{-1} penicillin and 100 μg ml^{-1} streptomycin (all from Biological Industries, Beit Haemek, Israel). BALB/c male mice (8–12 weeks old) were obtained from the breeding colony of Tel Aviv University, Israel. Animals were inoculated intra-cutaneously with 5×10^5 SQ2 cells in 0.2 ml HBSS buffer (Biological industries, Beit Haemek, Israel) into the low lateral side of the back. A single ^{224}Ra-bearing wire source was inserted 7–20 days after tumor cell inoculation, when the tumor average lateral diameter was 6–15 mm. Wire insertion was performed using standard 2.5 mL syringes with 23G needles. The wires were loaded into the needle tip and manipulated into the tumor center by a plunger placed internally along the syringe axis. Animal care and experimentation were carried out in accordance with Tel Aviv University guidelines. All surgical and invasive procedures were held under anesthesia.

4.3. ^{212}Pb distribution inside the tumor—tumor dissection experiments

The most direct method for determining the distribution of ^{212}Pb inside a treated tumor consists of dissecting the tumor into a large number of small pieces having known masses and measuring them individually by a gamma counter. This simple procedure was performed on 10 SCC tumors, each treated with a single source, when their average lateral diameter was 8–15 mm. Tumors were removed 2–4 days after source insertion, frozen in dry ice with acetone and dissected by surgical blades to $\sim$2 mm thick vertical slices. Each slice was further cut into 5–15 mg pieces in a manner that preserved the spatial arrangement while avoiding cross contamination of activity, with frequent replacement of blades. The entire ensemble of samples (typically 100–200 pieces) was then measured by a well-type NaI gamma counter (LKB Wallac 1282 CompuGamma, Wallac, Finland) focusing on the ^{212}Pb 239-keV line. Each sample was measured several times over a typical period of 24–72 h. Since ^{224}Ra has a 241-keV (4.1%) gamma line, which cannot be separated from the ^{212}Pb 239-keV line (43.6%) with the Wallac detector, the time-dependent data were fitted with a linear combination of two exponentials (with ^{224}Ra and ^{212}Pb half-lives) to account for the possible presence of ^{224}Ra in the sample.

^{212}Pb specific activity was found to be highly peaked in the immediate vicinity of the source, falling by about two orders of magnitude over 2–3 mm. Figure 4 shows the cumulative fraction of ^{212}Pb as a function of the cumulated mass of tumor cuts (sorted by descending order of ^{212}Pb specific activity), averaged over the ten tumors dissected. Note that although the majority of ^{212}Pb is found over a few dozen mg, there is a considerable fraction of activity farther away from the source. For example, 10% of the total ^{212}Pb activity is found outside of

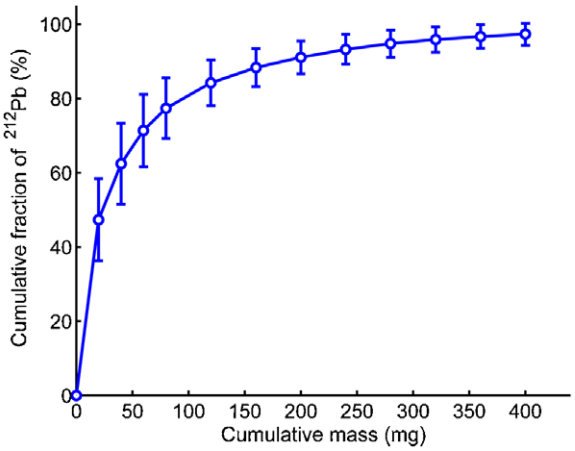

Figure 4. Results of tumor dissection experiments: the cumulative ^{212}Pb fraction inside the tumor as a function of the cumulative mass of tumor cuts, averaged over 10 SCC tumors dissected. Tumor cuts were sorted by their ^{212}Pb specific activity in descending order. Error bars represent standard deviations.

the central 200 mg region around the source. The typical amount of ^{224}Ra activity found in the dissected tumors was less than 1% of the ^{224}Ra source activity.

4.4. ^{212}Bi measurements by gamma spectroscopy

The possibility of ^{212}Bi redistribution relative to ^{212}Pb was studied on a macroscopic scale by gamma spectroscopy. The local activity ratio of ^{212}Bi and ^{212}Pb was evaluated for a series of 20–50 mg ($n = 15$) and 100–200 mg ($n = 11$) tumor cuts taken from three tumors treated with a single source, using a high resolution intrinsic germanium detector. The measurements, performed during the first 1–5 h after tumor removal (2–3 days after source insertion), used the characteristic gammas of ^{212}Bi—727 keV— and of its short-lived daughter ^{208}Tl—277 keV, 583 keV, 860 keV and 2615 keV. Each sample was measured 3–5 times for several minutes, at typical 1 h intervals. The time-dependent data were subsequently fitted with two exponentials (with ^{212}Pb and ^{212}Bi half-lives), yielding an estimate of the initial ^{212}Bi/^{212}Pb activity ratio. For the small tumor cuts (20–50 mg), the estimated ^{212}Bi/^{212}Pb activity ratio at the time of tumor removal was 1.03 ± 0.15 (range 0.84–1.33) and for the larger cuts (100–200 mg) -0.98 ± 0.08 (range 0.86–1.10). Both results are very close to 1.01, the theoretical value when the isotopes are in secular equilibrium driven by ^{224}Ra. Thus, ^{212}Bi redistribution relative to ^{212}Pb can be assumed to be a rather small effect.

4.5. ^{212}Pb autoradiography using a Fuji phosphor-imaging plate

The dissection method has the advantage of providing a straightforward measurement of the average ^{212}Pb activity in each tumor cut. However, the obtained spatial resolution is limited to about 2 mm. A 10-fold increase in resolution can be obtained by performing autoradiography measurements of ^{212}Pb in histological tumor cuts on a Fuji phosphor-imaging plate (Amemiya and Miyahara 1988). Note that rather than directly measuring ^{212}Pb itself, this procedure primarily records the alpha decays of ^{212}Bi and ^{212}Po which are generated by and are in local

secular equilibrium with ^{212}Pb, with only a minor contribution coming from the beta decays of ^{212}Pb.

In the experiments, ten SCC tumors were treated with a single source upon reaching a size of 6–15 mm. 2–7 days later the tumors were excised and the source removed. Excised tumors were placed in 4% formaldehyde for varying durations (overnight, 24, 36 or 48 h). The preserved specimens were processed and embedded in paraffin following standard procedures. Histological sections (5 or 10 μm) were cut using a Leica RM2055 microtome (Leica, Nussloch, Germany) and placed on glass slides. The slides were then laid on a Fuji imaging plate (BAS-TR2040S, Fuji Photo Film, Japan) over a 12 μm Mylar foil to prevent direct contact with the plate. Slides were measured twice, first for 2–3 h and then for about 15 h. In some cases a third measurement was performed on the following day. Following each measurement, the plate was scanned by a Fuji FLA-2000 system with a pixel size of either 100 or 200 μm. The specimens were later stained with Hematoxylin-Eosin (H&E) (Surgipath, Richmond, IL, USA) for tissue damage detection, to be correlated with the activity distribution measurements.

The images produced by scanning the imaging plate are a convolution of the actual activity patterns in the histological samples and the point spread function (PSF) of the plate (Bourgeois *et al* 1994, Kiss *et al* 2002). This results in some spreading, which can be corrected by applying deconvolution algorithms which usually require knowledge of the PSF. In our case, the recorded pattern was deconvoluted by applying the Lucy–Richardson algorithm (Lucy 1974, Richardson 1972) supplied in MATLAB's image processing toolbox. The procedure relied on separate measurements of the imaging plate PSF, using a point-like ^{212}Pb sample. Consecutive measurements of a given section were used to estimate the ^{224}Ra/^{212}Pb activity ratio in the histological sample by a dual-exponent fit. The deconvoluted image was converted pixel-wise to local ^{212}Pb activity (at the time the measurement began) using ^{212}Pb calibration samples of known activities measured concurrently with the histological sections. The local ^{212}Pb activity at the time of tumor removal was evaluated by back-extrapolation using the estimated ^{224}Ra/^{212}Pb ratio rather than assuming pure ^{212}Pb temporal behavior.

Analysis of the recorded images showed that the migration of ^{212}Pb inside the tumor (for sources placed near its center) was not isotropic, but anisotropy effects were generally not very large. ^{212}Pb activities were sharply peaked near the insertion point of the source, with considerable local activities extending over a region of several millimeters. In many cases the activity pattern appeared to spread towards the tumors periphery. *The observed activity patterns were consistent in neighboring sections and did not depend on the direction of the cutting procedure or the orientation of the section on the imaging plate*. The ^{224}Ra activity detected in the measured samples, 24–48 h after tumor removal, was typically a few per cent of the measured ^{212}Pb activity. The corresponding ^{224}Ra/^{212}Pb activity ratio at the time of tumor removal was about 1% or less, the same as in the tumor dissection experiments.

4.6. The ^{212}Bi/^{212}Po absorbed dose calculation

To obtain a rough estimate of the local dose contributed by the alpha decays of ^{212}Bi and ^{212}Po from source insertion until any given time (in particular, tumor removal or infinity), we adopted a simplified approach based on the following assumptions: (1) the biological settings affecting the diffusing atoms migration remain unchanged during the treatment; (2) the ^{212}Pb time dependence at any tumor point does not depend on its distance from the source; (3) ^{212}Bi and ^{212}Pb are identically distributed.

With this set of assumptions, one can estimate the local ^{212}Pb activity at all times, $\Gamma^j_{\mathrm{Pb}}(t)$ (where j is an index specifying the tumor cut or 'voxel'), *from a single measurement* $\Gamma^j_{\mathrm{Pb}}(t_r)$

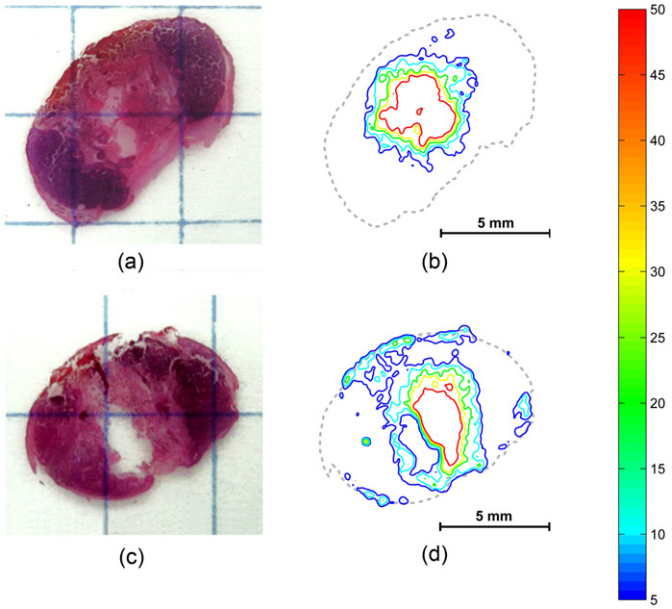

Figure 5. Calculated absorbed dose distributions, based on autoradiography measurements with a Fuji phosphor-imaging plate, compared to tissue damage in 10 μm H&E-stained histological sections taken from two SCC tumors. The scale refers to the alpha particle dose delivered by ^{212}Bi and ^{212}Po from source insertion until tumor removal (Gy). The dose curves shown; 5, 10, 20, 30 and 50 Gy.

at the time of tumor removal (appendix B). The assumption that ^{212}Bi redistribution can be neglected implies that each ^{212}Pb decay leads to a single alpha particle (of either ^{212}Bi or ^{212}Po) at the same location. Hence, the local absorbed dose (or actually, as noted above, kerma) from source insertion until time t, resulting from ^{212}Bi/^{212}Po alpha decays at the volume element j, is given by

$$\mathrm{Dose}^{j}_{\mathrm{BiPo}}(t) = \frac{E_{\mathrm{BiPo}}}{m_j}\int_0^t \Gamma^{j}_{\mathrm{Pb}}(t')\,\mathrm{d}t' \tag{1}$$

where E_{BiPo} is the average kinetic energy of the alpha particle emitted by either isotopes (7.8 MeV) and m_j is the mass of the jth tumor element. In the Fuji autoradiography experiments the 'voxel' mass was estimated by arbitrarily assuming a tissue density of 1.05 g cm^{-3}, using the pixel area and nominal section thickness to calculate the volume. The absorbed dose was calculated either from source insertion to infinity (asymptotic dose) or from source insertion until tumor removal. Approximate comparison between the estimated absorbed dose and the apparent tissue damage was performed by overlaying the calculated isodose curves of a given histological section on a scaled photograph of the same section (after H&E staining). Figure 5 depicts side by side the measured isodose curves and H&E-staining patterns of representative 10 μm histological sections taken from the central region of two treated tumors. The first tumor (a), (b) was treated with a 30 kBq ^{224}Ra source and the second (c), (d) with a 72 kBq ^{224}Ra source. ^{220}Rn desorption probabilities were 38% and 40%, respectively. The tumors were removed 4 and 5 days, respectively, after source insertion. The color-bar gives the scale for the calculated absorbed ^{212}Bi/^{212}Po alpha dose (in Gy) at the time of tumor removal (dose levels higher than 50 Gy are not shown; in the immediate vicinity of the source the dose rises to several thousand Gy). In both tumors necrotic areas are apparent around the

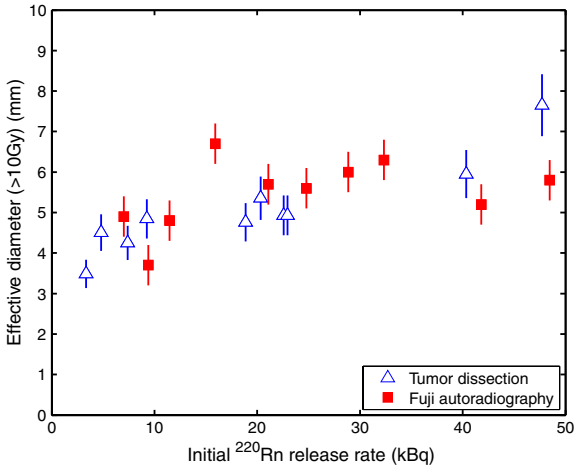

Figure 6. Results of tumor dissection and Fuji autoradiography experiments: dependence of the size of the region exposed to a calculated ^{212}Bi/^{212}Po asymptotic dose >10 Gy on source activity (initial release rate of ^{220}Rn).

source insertion point (where the calculated dose is maximal). The boundaries of the necrotic regions correspond to less than 1 Gy in the first tumor and about 5 Gy in the second. Similar comparisons performed on sections taken from other tumors (as well as on additional sections taken from the above two tumors) showed that the boundaries of the apparent necrotic regions corresponded to doses ranging from about 1 to 15 Gy. In all cases, there was good visual correspondence between the calculated dose and patterns of necrosis. Finally we note that *no cell damage was observed in the stained histological sections taken from SCC tumors treated with inert wires*.

4.7. Size of the affected region

In both types of ^{212}Pb distribution measurements we estimated the size (effective diameter) of the region receiving an asymptotic alpha-particle dose exceeding the reference value of 10 Gy. In the tumor dissection experiments, this was done by summing the masses of all cuts for which the calculated asymptotic dose exceeded 10 Gy, assuming that the total mass is spherical and calculating its diameter. In the Fuji autoradiography experiments, we chose a tumor section lying close to the source tip, summed the areas of all pixels for which the calculated asymptotic dose exceeded 10 Gy, assumed the total area was circular and took its diameter.

The effective diameter calculated from the tumor dissection experiments described above is somewhat overestimated, because the procedure involves averaging a steeply descending spatial distribution over $\sim$2 mm cuboids. The extent of this overestimate was assessed by separate calculations (not shown) which simulated the procedure by dividing the 3D space around a point source releasing diffusing ^{212}Pb atoms into cuboids whose sides were selected randomly from normal distributions representing the experimental ones. It was found that actual effective diameters were smaller by a factor of roughly 0.85 ± 0.10 than those calculated in the simulated dissection procedure. Thus, the effective diameters calculated from the dissection experiments were multiplied by this factor to obtain more realistic estimates.

Figure 6 summarizes the results from both tumor dissection and Fuji autoradiography experiments. The effective diameter dependence on the source activity is qualitatively similar

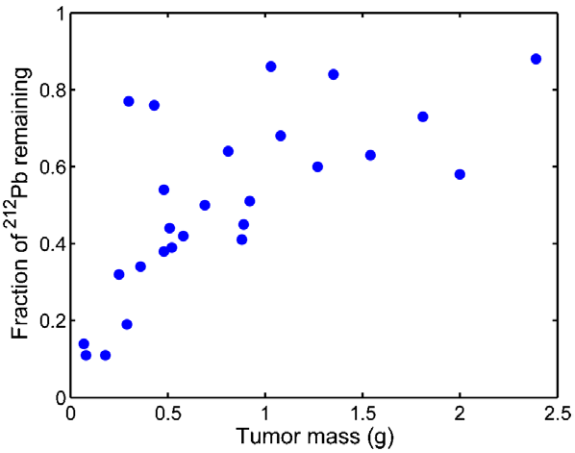

Figure 7. Fraction of ^{212}Pb remaining inside the tumor as a function of tumor mass. Typical uncertainties (not shown) are ±0.01.

to the theoretical prediction concerning the dose contributed by ^{220}Rn and ^{216}Po (figure 3(b)). Choosing 20 Gy as the reference dose, rather than 10 Gy, results in a similar effective diameter curve with all values lower by about 10%. The error bars in figure 6 represent the uncertainty in the correction factor applied to the results of the tumor dissection experiments, and the uncertainties related to the deconvolution procedure in the Fuji autoradiography experiments. Variations in the calculated effective diameters in neighboring sections, or variations resulting from uncertainties in the section ^{224}Ra content, were generally much smaller.

4.8. ^{212}Pb leakage and uptake by major organs

As noted above, the half-life of ^{212}Pb is sufficiently long to result in partial clearance from the tumor through the blood with subsequent uptake in various organs. The amount of ^{212}Pb leaking out of the tumor was found by calculating the total ^{212}Pb activity generated by the source and subtracting the ^{212}Pb activities inside the tumor and on the source itself. This required measuring the ^{212}Pb and ^{224}Ra activities on the source upon its removal from the tumor and the ^{212}Pb activity inside all tumor cuts using the Wallac gamma detector.

The ^{212}Pb leakage probability was measured for 26 SCC tumors with masses in the range 0.07–2.39 g, 2–12 days after being treated with a single source inserted to their center (of the 26 tumors measured, 22 were removed 2–5 days after source insertion). In all cases both tumor and source ^{212}Pb content was measured. ^{212}Pb measurements were also performed on several excised major organs as well as on blood samples. In several cases, samples were taken from the tumor bedding (immediately below the tumor).

As one might expect, the total ^{212}Pb leakage from the tumor, for a source placed roughly in its center, was found to depend on the tumor size, decreasing from up to about 90% for 0.1 g tumors to 12% for 2.4 g tumors. Alternatively, the fraction of ^{212}Pb remaining in the tumor increased from 10% to 88% over the same tumor mass range (figure 7).

^{212}Pb leaking from the tumor was found in all measured organs, in varying amounts which generally decreased with tumor mass. The largest ^{212}Pb concentration was detected, in all cases, in the kidneys. The absorbed fraction of ^{212}Pb (relative to the total amount of ^{212}Pb leaving the tumor) in the kidneys, liver, spleen, lungs and heart is shown in table 1. Also

Table 1. Fraction of leaked ^{212}Pb absorbed in the selected organs and ^{212}Pb concentration (activity per organ mass) relative to that found in the kidneys.

	Absorbed fraction of ^{212}Pb		Relative ^{212}Pb concentration
	Number of cases	Average ± SD	Average ± SD
Kidneys	26	8.5 ± 5.8%	1
Liver	25	4.9 ± 2.9%	0.21 ± 0.05
Lungs	22	0.5 ± 0.3%	0.13 ± 0.05
Spleen	22	0.4 ± 0.2%	0.11 ± 0.10
Heart	10	0.10 ± 0.06%	0.05 ± 0.04

shown is the ratio between ^{212}Pb concentration (^{212}Pb activity divided by organ mass) in the above organs relative to the ^{212}Pb concentration in the kidneys. Blood samples taken from seven animals showed that the overall blood content of ^{212}Pb was 1–7% of the entire ^{212}Pb activity leaving the tumor (with more than 95% of the activity in the red blood cells). Sporadic measurements of additional organs (stomach, intestines, colon, pancreas, urinary bladder, muscle, brain) yielded ^{212}Pb concentration in the range 0.01–0.13 of that of the kidneys.

Samples taken from adjacent tissue (in particular, the tumor bedding) contained minute ^{212}Pb activities, with the same typical concentration of other soft tissues (a few per cent of the kidney dose).

5. Discussion

5.1. Present study

The experimental results verify the basic premise of the proposed method, namely that the released atoms migrate to considerable distances from the source, giving rise to a substantial dose over a region measuring several millimeters. The somewhat anisotropic shapes of the observed activity patterns and necrotic regions apparently indicate that the dispersion of alpha emitters throughout the tumor is affected by convective processes (either vascular or interstitial) and is not dependent on simple diffusion mechanisms only.

DART is similar, in a sense, to intralesional targeted alpha therapy. Both methods attempt to bypass physical obstacles that hinder the effective dispersion of the targeting vectors in systemic α-RIT, in particular those related to their extravasation from the blood, by allowing the radionuclides to begin their journey in the cellular space. The fact that DART does not rely on a molecular targeting mechanism is, on the one hand, a limitation as healthy cells may also become subject to alpha particle irradiation; on the other hand, it may also facilitate the migration of alpha emitters inside the tumor, as they do not bind to cellular targets in the immediate vicinity of the source. In addition, DART may offer a practical way of covering the tumor volume with a known (and relatively stable) geometry of sources, enabling, in principle, approximate treatment planning and post-implantation treatment evaluation.

The dose calculation scheme presented in this paper should be regarded merely as an approximate method of providing rough estimates of the size and shape of the affected region. The central assumption of this model that the properties of the medium are time-independent is a crude one, since, in particular, the vascular network in the immediate surrounding of the source is likely affected by its presence. This assumption can hold, however, in regions of low vascularity, for example in central regions of large tumors. The assumption that the temporal behavior of ^{212}Pb is identical at all points throughout the tumor implicitly neglects

any delay that may result from the finite time it takes the atoms (in whatever chemical form) to traverse the tissue. This, however, may not be in gross error, since such delays are expected to be of the order of minutes or several hours at most—much shorter than the duration of the treatment (days). The assumption that ^{212}Bi is in local secular equilibrium with ^{212}Pb is justified (macroscopically) by the experimental data. Our calculations do not account for the difference between kerma and absorbed dose and for possible variations of the LET along the track of the alpha particles, as these are second-order effects. Note that even if the errors in the estimated dose are as high as 100%, the resulting changes in the calculated effective diameters are at most 0.5–1 mm.

The rationale for choosing 10 Gy as the reference dose for which to estimate the size of the affected region is as follows. Tumors can usually be eradicated by a single fraction of photons amounting to a typical dose of 20–25 Gy (i.e., 20–25 Sv); since alpha particles impart irreparable damage to the DNA (and their effect is nearly independent of the oxygenation state of the cell), the required dose equivalent in alpha particle-based treatments should thus be roughly the same. Assuming a modest relative biological effectiveness (RBE) of two, an alpha particle dose of about 10 Gy should achieve this. In addition, if DART sources are arranged on a lattice (e.g. hexagonal) with a typical spacing which equals the 'diameter' of the region receiving >10 Gy, the minimal dose in the lattice can safely be expected to exceed $\sim$20 Gy, even if significant anisotropic convective effects are involved. Thus the 10 Gy 'effective diameter' can serve as a guide for the required intra-source spacing in DART wire lattices. Note that for SQ2 derived tumors, where the typical cross section of the nucleus is 40–50 μm^2, the average number of alpha particle traversals through a given nucleus in a 10 Gy region is about 15–25. Assuming Poisson statistics and an average of 15 traversals, the probability that a given nucleus is not traversed by alpha particles is 3×10^{-7}, while its probability to be hit by more than 3 is 0.9998.

The histological observation that cell death extends, in some cases, to regions of very low calculated doses, may reflect inaccuracies in the approximate dose calculation scheme. However, it may also indicate that some of the damage imparted to the tissue results from secondary effects, such as damage to the tumor vasculature that deprives cells from oxygen and nutrients. This intriguing question is left for future research.

The large fraction of ^{212}Pb remaining inside the tumor indicates that its typical removal time is of the order of several hours, with shorter times corresponding to smaller tumors. The presence of ^{212}Pb in all of the measured organs, as well as inside the blood, clearly verifies that ^{212}Pb leaves the tumor through the vascular network. Prolonged removal times may result from the time it takes a ^{212}Pb-labeled protein to diffuse to a viable blood vessel (particularly in the necrotic vicinity of the source), as well as from the chaotic and leaky nature of the tumoral vascular network, with its many loops and dead-ends.

The size of the region affected by ^{212}Bi and ^{212}Po is apparently larger than that of the region affected by ^{220}Rn and ^{216}Po. Thus, it is possible that the dose contributed by ^{220}Rn and ^{216}Po is 'wasted' over a region that absorbs, in any case, a sufficiently high dose from the decays of ^{212}Bi and ^{212}Po. The contribution of the alpha decays of ^{220}Rn and ^{216}Po may become more important, though, in highly vascular regions where, on the one hand, ^{212}Pb removal times will be short and, on the other, the dispersion of ^{220}Rn may be enhanced. In addition, ^{220}Rn possibly plays, because of its inert nature, a vital role in the initial dispersion of ^{212}Pb near the source, enabling it to begin its journey all across the cellular space. We note, for completeness, that numerical calculations (not shown) indicated that the dose delivered by the beta decays of ^{212}Pb, ^{212}Bi and ^{208}Tl is limited to the close vicinity (a radius of 1–1.5 mm) of the source and is completely masked by the alpha particle dose delivered by the diffusing atoms.

5.2. Future considerations

This paper focused on the physical principles of DART. Extensive work demonstrating the efficacy of DART against experimental tumor models in mice, with respect to both tumor development and life expectancy, is described elsewhere (Cooks *et al* 2007). Work addressing the dispersion of ^{224}Ra daughters in additional tumor models is under way.

The possible utilization of DART in the treatment of human patients will evidently call for the application of multiple ^{224}Ra sources. This will obviously require careful consideration of the accumulation of ^{212}Pb leaking out of the tumor in healthy organs. Extensive internal dosimetry assessment calculations (to be described in detail elsewhere), based on the ICRP biokinetic model for lead (ICRP 1993, Leggett 1993) and the OLINDA code (Stabin *et al* 2005), demonstrate that the dose to all organs can be expected to lie well below limiting tolerance levels even when the treatment of relatively large tumors is considered. For example, assuming the application of 200–400 kBq (about 5–10 μCi) ^{224}Ra per tumor gram, the alpha particle dose to the bone surface and kidneys (the organs which receive the highest calculated dose) when treating a 3 cm diameter spherical tumor will be 0.1–0.2 Gy. The red marrow, in this case, will receive an alpha particle dose about five times lower. Because of the low activities involved, gamma emissions along the chain are negligible with respect to the safety of both patient and medical staff. One should note, however, that the dose delivered to distant organs as a result of ^{212}Pb uptake may limit the scope of DART treatments to patients diagnosed with a small number of localized tumors.

Regarding the applicability of the method, the ^{224}Ra decay chain has several attractive features: (1) ^{228}Th is readily available; (2) ^{228}Th half-life (1.91 y) is long enough for sustained source production from a given generator; (3) ^{224}Ra half-life (3.66 d) is, on the one hand, long enough from a logistic point of view (i.e., sources can be prepared at a remote facility and shipped with minimal loss of activity) and, on the other hand, short enough to deliver the therapeutic dose over a short period of time. Finally, the source preparation procedure is simple and easily scalable.

To conclude, the observation that a single DART source generates a region of high radiation dose and extensive cell death measuring millimeters in size, coupled with the low activities involved and the simplicity of source preparation, combine to suggest that DART may potentially become an effective and safe tool in the treatment of solid tumors.

Acknowledgments

This work was partially supported by the Horowitz-Ramot fund and Althera Medical Ltd.

Appendix A. ^{220}Rn/^{216}Po dose calculation

We assume that ^{220}Rn atoms are released from a point source at the origin, at a rate $S(t) = S(0)\,\mathrm{e}^{-\lambda_{\mathrm{Ra}}t}$. $S(0)$ is the ^{220}Rn release rate at the moment of source insertion into the tumor and λ_{Ra} is the ^{224}Ra decay constant ($\lambda_{\mathrm{Ra}} = 2.19 \times 10^{-6}$ s^{-1}). The time-dependent diffusion equation describing the spatial concentration of ^{220}Rn atoms, $n_{\mathrm{Rn}}(r, t)$ (atoms cm^{-3}) is

$$\frac{\partial n_{\mathrm{Rn}}}{\partial t} = D_{\mathrm{Rn}}\nabla^2 n_{\mathrm{Rn}} - \lambda_{\mathrm{Rn}} n_{\mathrm{Rn}} \qquad \text{for} \quad r > 0 \tag{A.1}$$

with the boundary condition at $r = 0$:

$$\lim_{r\to 0} 4\pi r^2 j_{\mathrm{Rn}}(r, t) = S(0)\,\mathrm{e}^{-\lambda_{\mathrm{Ra}}t} \tag{A.2}$$

where $j_{\mathrm{Rn}}(r,t) = -D_{\mathrm{Rn}}\frac{\partial n_{\mathrm{Rn}}}{\partial r}$ is the (radial) current density of ^{220}Rn (atoms cm^{-2} s^{-1}), D_{Rn} is radon's effective diffusion coefficient, λ_{Rn} is the ^{220}Rn decay constant ($\lambda_{\mathrm{Rn}} = 0.0125$ s^{-1}) and ∇^2 is the Laplacian operator.

Within several half-lives of ^{220}Rn the solution for equation (A.1) stabilizes on the asymptotic form:

$$n_{\mathrm{Rn}}(r,t) = \frac{S(0)\,\mathrm{e}^{-\lambda_{\mathrm{Ra}}t}}{4\pi D_{\mathrm{Rn}}} \cdot \frac{\mathrm{e}^{-r/L_{\mathrm{Rn}}}}{r} \tag{A.3}$$

where $L_{\mathrm{Rn}} = \sqrt{D_{\mathrm{Rn}}/(\lambda_{\mathrm{Rn}} - \lambda_{\mathrm{Ra}})}$ is the diffusion length of ^{220}Rn. Neglecting the initial buildup phase of ^{220}Rn, the asymptotic dose (from source insertion to infinity) resulting from the alpha decays of ^{220}Rn and ^{216}Po is

$$D_{\infty}(r) = \frac{1}{\rho}\int_0^{\infty} \lambda_{\mathrm{Rn}} n_{\mathrm{Rn}}(r,t)\cdot(E_{\mathrm{Rn}} + E_{\mathrm{Po}})\,\mathrm{d}t \approx \frac{\lambda_{\mathrm{Rn}} S(0)\,\mathrm{e}^{-r/L_{\mathrm{Rn}}}\tau_{\mathrm{Ra}}\cdot(E_{\mathrm{Rn}} + E_{\mathrm{Po}})}{4\pi\rho D_{\mathrm{Rn}} r} \tag{A.4}$$

where $\tau_{\mathrm{Ra}} = 1/\lambda_{\mathrm{Ra}}$, E_{Rn} and E_{Po} are the kinetic energies of the alpha particles emitted by ^{220}Rn and ^{216}Po (6.288 MeV and 6.778 MeV, respectively) and ρ is the tissue density (here assumed 1.05 g cm^{-3}).

Appendix B. ^{212}Bi/^{212}Po dose calculation

Let $N^j_{\mathrm{Pb}}(t)$ be the total number of ^{212}Pb atoms inside an element j at time t. We assume that each decay event of ^{224}Ra on the source *immediately* gives rise to f_j new ^{212}Pb atoms in element j (no time delays) and that f_j *is not time dependent* (fixed biological settings). Hence,

$$\frac{\mathrm{d}N^j_{\mathrm{Pb}}}{\mathrm{d}t} = f_j\Gamma^{src}_{\mathrm{Ra}}(t) - \lambda_{\mathrm{Pb}}N^j_{\mathrm{Pb}}. \tag{B.1}$$

Equation (B.1) gives, for the local ^{212}Pb activity (taking $\Gamma^j_{\mathrm{Pb}}(0) = 0$),

$$\Gamma^j_{\mathrm{Pb}}(t) = f_j\frac{\lambda_{\mathrm{Pb}}}{\lambda_{\mathrm{Pb}} - \lambda_{\mathrm{Ra}}}\Gamma^{src}_{\mathrm{Ra}}(0)\cdot\left(\mathrm{e}^{-\lambda_{\mathrm{Ra}}t} - \mathrm{e}^{-\lambda_{\mathrm{Pb}}t}\right). \tag{B.2}$$

Specifically, at the time of tumor removal,

$$\Gamma^j_{\mathrm{Pb}}(t_r) = f_j\frac{\lambda_{\mathrm{Pb}}}{\lambda_{\mathrm{Pb}} - \lambda_{\mathrm{Ra}}}\Gamma^{src}_{\mathrm{Ra}}(0)\cdot\left(\mathrm{e}^{-\lambda_{\mathrm{Ra}}t_r} - \mathrm{e}^{-\lambda_{\mathrm{Pb}}t_r}\right). \tag{B.3}$$

Thus, by dividing the above two equations, the local activity at time t can be calculated based on the *measured* activity at the time of tumor removal:

$$\Gamma^j_{\mathrm{Pb}}(t) = \Gamma^j_{\mathrm{Pb}}(t_r)\frac{\mathrm{e}^{-\lambda_{\mathrm{Ra}}t} - \mathrm{e}^{-\lambda_{\mathrm{Pb}}t}}{\mathrm{e}^{-\lambda_{\mathrm{Ra}}t_r} - \mathrm{e}^{-\lambda_{\mathrm{Pb}}t_r}}. \tag{B.4}$$

We now turn to calculate the dose. The assumption that there is no redistribution of ^{212}Bi implies that each decay event of ^{212}Pb leads to a single alpha particle emission at the same location. Neglecting the $\sim$1 h delay between the decay events of ^{212}Pb and ^{212}Bi, the dose at time t is given by

$$\begin{aligned}\mathrm{Dose}^j_{\mathrm{BiPo}}(t) &= \frac{E_{\mathrm{BiPo}}}{m_j}\int_0^t \Gamma^j_{\mathrm{Pb}}(t')\,\mathrm{d}t' \\ &= \frac{E_{\mathrm{BiPo}}}{m_j}\cdot\frac{\Gamma^j_{\mathrm{Pb}}(t_r)}{\mathrm{e}^{-\lambda_{\mathrm{Ra}}t_r} - \mathrm{e}^{-\lambda_{\mathrm{Pb}}t_r}}\left(\tau_{\mathrm{Ra}}\cdot\left(1 - \mathrm{e}^{-\lambda_{\mathrm{Ra}}t}\right) - \tau_{\mathrm{Pb}}\cdot\left(1 - \mathrm{e}^{-\lambda_{\mathrm{Pb}}t}\right)\right)\end{aligned} \tag{B.5}$$

where $\tau_{Ra} = 1/\lambda_{Ra}$, $\tau_{Pb} = 1/\lambda_{Pb}$ and m_j is the mass element j. The asymptotic dose is

$$\mathrm{Dose}^{j}_{\mathrm{BiPo}}(\infty) = \frac{E_{\mathrm{BiPo}}}{m_j}\int_0^{\infty}\Gamma^{j}_{\mathrm{Pb}}(t')\,\mathrm{d}t' = \frac{E_{\mathrm{BiPo}}}{m_j}\cdot\frac{\Gamma^{j}_{\mathrm{Pb}}(t_r)\cdot(\tau_{\mathrm{Ra}}-\tau_{\mathrm{Pb}})}{\mathrm{e}^{-\lambda_{\mathrm{Ra}}t_r}-\mathrm{e}^{-\lambda_{\mathrm{Pb}}t_r}}. \quad \text{(B.6)}$$

References

Allen B J 2006 Internal high linear energy transfer (LET) targeted radiotherapy for cancer *Phys. Med. Biol.* **51** R327–41

Allen B J *et al* 2005 Intralesional targeted alpha therapy for metastatic melanoma *Cancer Biol. Ther.* **4** 1318–24

Allen B J, Rizvi S M A and Tian Z 2001 Preclinical targeted alpha therapy for subcutaneous melanoma *Melanoma Res.* **11** 175–82

Amemiya Y and Miyahara J 1988 Imaging plate illuminates many fields *Nature* **336** 89–90

Blank M, Lavie G, Mandel M, Hazan S, Orenstein A, Meruelo D and Keisari Y 2004 Antimetastatic activity of the photodynamic agent hypericin in the dark *Int. J. Cancer* **111** 596–603

Bourgeois D, Moy J P, Svensson S O and Kvick Å 1994 The point-spread function of X-ray image-intensifiers/CCD-camera and imaging-plate systems in crystallography: assessment and consequences for the dynamic range *J. Appl. Cryst.* **27** 868–77

Christiansen J and Rajasekaran A K 2004 Biological impediments to monoclonal antibody-based cancer immunotherapy *Mol. Cancer Ther.* **3** 1493–501

Cooks T, Arazi L, Schmidt M, Keisari Y and Kelson I 2007 Growth retardation and destruction of experimental squamous cell carcinoma by interstitial radioactive wires releasing diffusing alpha-emitting atoms *Int. J. Cancer* Submitted

Couturier O, Supiot S, Degraef-Mougin M, Faivre-Chauvet A, Carlier T, Chatal J F, Davodeau F and Cherel M 2005 Cancer radioimmunotherapy with alpha-emitting nuclides *Eur. J. Nucl. Med. Mol. Imaging* **32** 601–14

Godwin H A 2001 The biological chemistry of lead *Curr. Opin. Chem. Biol.* **5** 223–7

Hall E J 2000 *Radiobiology for the Radiologist* 5th edn (Philadelphia, PA: Lippincott Williams & Wilkins)

ICRP 1993 Age-Dependent Doses to Members of the Public from Intake of Radionuclides: Part 2 Ingestion Dose Coefficients *ICRP Publication 67 Ann. of the ICRP vol 23 (3-4)* (Oxford: Pergamon)

Jahne B, Heinz G and Dietrich W J 1987 Measurement of the diffusion coefficients of sparingly soluble gases in water *J. Geophys. Res.* **92** 10767–76

Jain R K 1999 Transport of molecules, particles and cells in solid tumors *Ann. Rev. Biomed. Eng.* **1** 241–63

Jain R K and Baxter L T 1988 Mechanisms of heterogeneous distribution of monoclonal antibodies and other macromolecules in tumors: significance of elevated interstitial pressure *Cancer Res.* **48** 7022–32

Jurcic J G 2005 Immunotherapy for acute myeloid leukemia *Curr. Oncol. Rep.* **7** 339–46

Kennel S J, Boll R, Stabin M, Schuller H M and Mirzadeh S 1999 Radioimmunotherapy of micrometastases in lung with vascular targeted ^{213}Bi *Br. J. Cancer* **80** 175–84

Kiss M Z, Sayers D E and Zhong Z 2002 Comparison of x-ray detectors for a diffraction enhanced imaging system *Nucl. Instrum. Methods* B **491** 280–90

Kneifel S *et al* 2006 Local targeting of malignant gliomas by the diffusible peptidic vector 1,4,7,10-tetraazacyclododecane-1-glutaric acid-4,7,10-triacetic acid-substance p *Clin. Cancer Res.* **12** 3843–50

Larsen R H, Akabani G, Welsh P and Zalutsky M R 1998 The cytotoxicity and microdosimetry of astatine-211-labeled chimeric monoclonal antibodies in human glioma and melanoma cells in vitro *Radiat. Res.* **149** 155–62

Larsen R H and Bruland O S 1998 Intratumor injection of immunoglobulins labelled with the alpha-particle emitter ^{211}At: analyses of tumor retention, microdistribution and growth delay *Br. J. Cancer* **77** 1115–22

Lederer C M and Shirley V S 1977 *Table of Isotopes* 7th edn (New York: Wiley)

Leggett R W 1993 An age-specific kinetic model of lead metabolism in humans *Environ. Health Perspect.* **101** 598–616

Lucy L B 1974 An iterative technique for the rectification of observed distributions *Astron. J.* **79** 745–54

Macklis R M, Lin J Y, Beresford B, Atcher R W, Hines J J and Humm J L 1992 Cellular kinetics, dosimetry, and radiobiology of alpha-particle radioimmunotherapy: induction of apoptosis *Radiat. Res.* **130** 220–6

Mulford D A, Scheinberg D A and Jurcic J G 2005 The promise of targeted alpha-particle therapy *J. Nucl. Med.* **46** (Suppl.) 199S–204S

Nilsson S, Larsen R H, Fossa S D, Balteskard L, Borch K W, Westlin J E, Salberg G and Bruland O S 2005 First clinical experience with alpha-emitting radium-223 in the treatment of skeletal metastases *Clin. Cancer Res.* **11** 4451–9

NRC 1999 *Risk Assessment of Radon in Drinking Water* (Washington, DC: National Academy Press)

Richardson W H 1972 Bayesian-based iterative method of image restoration *J. Opt. Soc. Am.* **62** 55–9

Rotmensch J, Atcher R W, Hines J, Toohill M and Herbst A L 1989 Comparison of short-lived high-LET alpha-emitting radionuclides lead-212 and bismuth-212 to low-LET X-rays on ovarian carcinoma *Gynecol. Oncol.* **35** 297–300

Schmidt D *et al* 2004 Phase I clinical study on alpha-therapy for non Hodgkin lymphoma *Proc. 4th Alpha-immunotherapy Symp., (Düsseldorf, Germany, June 28–29)* ed A Morgenstern

Stabin M G, Sparks R B and Crowe E 2005 OLINDA/EXM: the second-generation personal computer software for internal dose assessment in nuclear medicine *J. Nucl. Med.* **46** 1023–27

Zalutsky M R 2005 Current status of therapy of solid tumors: brain tumor therapy *J. Nucl. Med.* **46** (Suppl.) 151S–156S

Zalutsky M R 2006 Targeted α-particle therapy of microscopic disease: providing a further rationale for clinical investigation *J. Nucl. Med.* **47** 1238–40